


ORIGINAL ARTICLE

Hydraulic acclimation in a Mediterranean oak subjected to permanent throughfall exclusion results in increased stem hydraulic capacitance

Roberto L. Salomón¹  | Kathy Steppe¹ | Jean M. Ourcival² | Selwyn Villers¹ | Jesús Rodríguez-Calcerrada³ | Roderick Schapman¹ | Jean M. Limousin²

¹Laboratory of Plant Ecology, Department of Plants and Crops, Faculty of Bioscience Engineering, Ghent University, Ghent, Belgium

²Centre d'Ecologie Fonctionnelle et Evolutive (CEFE), CEFE UMR 5175, CNRS, Univ Montpellier, Univ Paul Valéry Montpellier 3, EPHE, IRD, Montpellier Cedex 5, France

³Forest Genetics and Ecophysiology Research Group, Universidad Politécnica de Madrid, Madrid, Spain

Correspondence

Roberto L. Salomón, Laboratory of Plant Ecology, Department of Plants and Crops, Faculty of Bioscience Engineering, Ghent University, Coupure links 653, 9000 Ghent, Belgium.

Email: robertoluis.salomonmoreno@ugent.be

Funding information

Ecofor, Allenvi, ANAEE-F, OSU-OREME, FWO and the European Union's Horizon 2020.

Abstract

Stem water storage capacity and hydraulic capacitance (C_s) play a crucial role in tree survival under drought-stress. To investigate whether C_s adjusts to increasing water deficit, variation in stem water content (StWC) was monitored in vivo for 2 years and related to periodical measurements of tree water potential in Mediterranean *Quercus ilex* trees subjected either to permanent throughfall exclusion (TE) or to control conditions. Seasonal reductions in StWC were larger in TE trees relative to control ones, resulting in greater seasonal C_s (154 and 80 kg m⁻³ MPa⁻¹, respectively), but only during the first phase of the desorption curve, when predawn water potential was above -1.1 MPa. Below this point, C_s decreased substantially and did not differ between treatments (<20 kg m⁻³ MPa⁻¹). The allometric relationship between tree diameter and sapwood area, measured via electrical resistivity tomography, was not affected by TE. Our results suggest that (a) C_s response to water deficit in the drought-tolerant *Q. ilex* might be more important to optimize carbon gain during well-hydrated periods than to prevent drought-induced embolism formation during severe drought stress, and (b) enhanced C_s during early summer does not result from proportional increases in sapwood volume, but mostly from increased elastic water.

KEYWORDS

capacitive water, carbon gain optimization, desorption curve, drought-stress, electrical resistivity tomography, frequency domain reflectometry, rainfall exclusion, sapwood area, stem water content, tree acclimation

1 | INTRODUCTION

In the early 20th century, Spalding (1905) reported for the first time clear evidence of stem water storage and related diameter changes for the Suaharo desert plant. Later studies described a significant imbalance between leaf transpiration and soil water uptake, and suggested an important role of water storage throughout plant tissues, mainly in the stem, to satisfy the evaporative demand under water limiting conditions (Kramer, 1937, and references therein). This pioneering work demonstrated that tree stems are not inert pipelines along the root-to-leaf

continuum. A more recent body of studies has since highlighted the physiological relevance of stem water pools in plant transpiration, hydraulic modelling and survival (Goldstein et al., 1998; Körner, 2019; Martínez-Vilalta, Anderegg, Sapes, & Sala, 2019; Meinzer, Johnson, Lachenbruch, McCulloh, & Woodruff, 2009; Salomón, Limousin, Ourcival, Rodríguez-Calcerrada, & Steppe, 2017; Scholz, Phillips, Bucci, Meinzer, & Goldstein, 2011; Steppe, De Pauw, Lemeur, & Vanrolleghem, 2006; Tyree & Yang, 1990; Waring & Running, 1978; Zweifel, Item, & Häsler, 2001). These studies have helped to more comprehensively understand drought-driven embolism formation and plant hydraulic functioning.

When a plant transpires, a gradient in water potential (Ψ) along the soil–plant–atmosphere continuum is generated. This vertical Ψ gradient results in a radial Ψ gradient between stem xylem conduits and surrounding tissues that drives a dynamic radial water flow within tree stems according to transpiration needs (Steppe, Sterck, & Deslauriers, 2015). As a result, stem water pools are depleted when the evaporative demand exceeds tree water uptake by the root system. Inversely, stem water pools are replenished when root water uptake exceeds tree transpiration until stem radial Ψ gradients reach hydraulic equilibrium. Under drought stress conditions, water tension in xylem conduits increases and the xylem functionality is endangered by the risk of embolism, which may hinder tree transpiration and carbon gain. Capacitive water release from tree stems buffers increases in xylem tension thereby delaying or avoiding embolism formation in situations of water limitation (Meinzer et al., 2008, 2009; Scholz et al., 2011; Vergeynst, Dierick, Bogaerts, Cnudde, & Steppe, 2015). Water release from stem tissues to the transpiration stream across a gradient of xylem Ψ is described by the stem desorption curve, theoretically divided into three phases (Pratt & Jacobsen, 2017; Steppe, 2018; Tyree & Ewers, 1991; Tyree & Yang, 1990). The first phase of this curve occurs at relatively high xylem Ψ , when the plant is well hydrated. Here, a relatively large amount of capillary water is released for a small change in xylem Ψ in a nearly linear manner. Capillary water is mostly located in intercellular spaces and open conduits (i.e., conduits with open ends), tracheids and fibres. The desorption curve flattens along the second phase as water is released at a slower rate for a comparatively large reduction in stem Ψ . Along this phase, water is primarily released from elastic living cells, integrating parenchyma, cambium and peridermal tissues. Finally, the desorption curve steepens during the third phase, when water is mostly released from embolized vessels or tracheids before total stem dehydration. The amount of water released at this point largely depends on the amount and lumen size of embolized conduits. Recent studies performed *in vivo* using X-ray microtomography question, however, whether this sequential release of capacitive water sources along the desorption curve, which has been derived from excised branches, can be extrapolated to living plants (Knipfer et al., 2017, 2019).

Stem hydraulic capacitance (C_s ; $\text{kg m}^{-3} \text{MPa}^{-1}$) is defined by the amount of stem water released (ΔW ; kg) for a given change in xylem water potential ($\Delta\Psi$; MPa) per unit of tissue volume (V ; m^3) (Tyree & Ewers, 1991):

$$C_s = \frac{\Delta W}{\Delta\Psi} \frac{1}{V} \quad (1)$$

Stem capacitance largely varies according to the stem water status (Salomón et al., 2017; Vergeynst et al., 2015). However, it is commonly estimated by the initial slope of the desorption curve (Barnard et al., 2011; McCulloh, Johnson, Meinzer, & Woodruff, 2014; Meinzer, James, Goldstein, & Woodruff, 2003; Vergeynst et al., 2015), when the stem is well hydrated. Stem storage capacity is largely determined by stem size (Meinzer, James, & Goldstein, 2004; Scholz et al., 2011), and more specifically, by sapwood volume (Goldstein

et al., 1998): the larger the tree, the more room for water storage. Moreover, beyond this intuitive relationship, larger trees seem to rely to a greater extent on stored water to fulfil transpiration needs (Phillips et al., 2003; Scholz et al., 2011) and thus have greater C_s (Domec & Gartner, 2001; McCulloh et al., 2014), although the underlying causes of a direct relation between C_s and sapwood volume remain unexplored. This suggests, nevertheless, that C_s might be a relatively plastic trait related to biomass allocation patterns: as trees grow and allocate most of their biomass to the stem (Poorter et al., 2012), the amount of conducting and storing biomass increases to the detriment of transpiring tissues (i.e., leaves).

A trade-off between C_s and xylem resistance to embolism has been reported, with “drought-avoidant” species characterized by low wood density and embolism-vulnerable xylem having large C_s , which dampens the reductions in xylem Ψ , and “drought-tolerant” species characterized by high wood density and xylem conduits able to maintain functionality at low Ψ having low C_s (McCulloh et al., 2014; Meinzer et al., 2008, 2009). Accordingly, evergreen sclerophyll species across an aridity gradient exhibited lower wood density, greater C_s and less negative xylem Ψ in high-rainfall sites (Richards, Wright, Lenz, & Zanne, 2014). This pattern, however, does not seem to hold at the intraspecific level. Comparisons in ponderosa pine and Douglas-fir showed that, for both species, trees growing in drier locations had greater C_s and sapwood thickness, and were more vulnerable to embolism formation (Barnard et al., 2011). These authors suggested that enhanced C_s under drier conditions may partially explain the lack of acclimation of structural traits related to the resistance of xylem to embolism, which has been demonstrated to be limited in intraspecific comparisons across aridity gradients (Lamy et al., 2014; Martínez-Vilalta et al., 2009; Rosas et al., 2019; Schuldt et al., 2016; Wortemann et al., 2011), as well as in manipulative experiments that alter soil water availability (Hudson et al., 2018; Limousin, Longepierre, Huc, & Rambal, 2010). On the other hand, structural adjustment of biomass allocation is a key strategy to optimize water use (Choat et al., 2018; Magnani, Grace, & Borghetti, 2002), and reductions of the leaf-to-sapwood area ratio are commonly reported as a mechanism to maintain homeostatic minimum stem Ψ , and hence hydraulic functionality, while supplying water to the canopy under drought stress (Martínez-Vilalta et al., 2009; Martin-StPaul et al., 2013; Mencuccini, 2003; Rosas et al., 2019; White, Beadle, Worledge, Honeysett, & Cherry, 1998).

The need for better considering the role of stem water pools and C_s in drought-driven tree mortality has recently been highlighted (Körner, 2019; Martínez-Vilalta et al., 2019). However, we still lack direct assessments on the effect of drought stress on C_s and related metrics. Permanent rainfall manipulations in the field provide an excellent opportunity to investigate long-term plant acclimation to increasing water limitation, as this approach allows straightforward comparison of the surveyed trait in the same species and at the same site, thus minimizing confounding co-factors that may vary over space and time. To advance our knowledge on stem water pools and hydraulic acclimation to drought stress, cutting-edge technologies were applied to measure *in vivo* stem water content (StWC), C_s , sap

flow and sapwood area (SA) in *Quercus ilex* trees subjected to control conditions and long-term, partial throughfall exclusion (TE) in a Mediterranean stand. Variation in StWC was continuously monitored for 2 years using frequency domain reflectometry (FDR), and SA was discretely measured applying electrical resistivity tomography. Based on a previous modelling exercise at the study site, in which the reliance on stored water to daily transpiration increased with drought stress (Salomón et al., 2017), and given that C_s is beneficial to buffer xylem Ψ reductions (Meinzer et al., 2009), we hypothesized that TE would enhance C_s , particularly under conditions of severe drought stress. If true, we expected that potential increases in C_s would be related to allometric adjustments reflected in the relationship between stem diameter and SA.

2 | MATERIALS AND METHODS

2.1 | Site study and experiment setup

The study was conducted in the Puéchabon State Forest (Occitanie, France), in an experimental plot dominated by *Q. ilex* (43°44,029'N, 3°35,045'E, 270 m.a.s.l.). The site was historically coppiced until 1942. Stand density is 4,700 stems/ha, average dominant height is 5.5 m and most stems (>70%) have a stem diameter at breast height (DBH) between 4 and 10 cm. Climate is Mediterranean with an annual mean temperature of 13.5°C and 953 mm of annual precipitation. Summer is hot and dry with less than 20% of the annual precipitation falling during this season. Air temperature, precipitation and relative humidity are measured in a weather station located in the experimental site (see, for example, Rambal et al., 2014 for further details on the site). A permanent partial TE experiment started in spring 2003 in three plots of 10 × 10 m; Rain gutters were suspended below the canopy at approximately 1.5 m above the soil in order to cover one third of the plot area and drive throughfall outside the plots. This experimental set-up was shown to effectively reduce the total net precipitation by 28% (Limousin, Rambal, Ourcival, & Joffre, 2008). In the control plots the same gutters were suspended upside down to avoid microclimatic differences between treatments (see Rodríguez-Calcerrada et al., 2011 for a photograph and further details on the TE setup). Four trees per treatment located within one of the replicate plots were selected in December 2016 to measure StWC, predawn and midday leaf Ψ , C_s as the reduction in StWC for a given drop in Ψ (see below) and stem sap flow. Stem DBH of selected trees did not differ between treatments ($p = .71$), with mean values of 11.40 ± 0.85 cm. Ten trees in each treatment were selected to measure SA across a wide range of stem DBH in spring 2019.

2.2 | Stem water content

StWC was monitored by FDR with GS3 moisture probes (Decagon Instruments, Pullman, WA) (Hao, James, Michele Holbrook, & Goldstein, 2013; Matheny et al., 2015; Oliva Carrasco et al., 2015).

According to the allometric relationship between stem diameter and SA previously observed at the experimental site (Equation (1) in Limousin et al., 2009), the estimated sapwood depth in monitored trees (3.25 ± 0.23 cm) was smaller than the probe needle length (5.5 cm). Probe needles were therefore shortened to 3 cm with a rotary tool to avoid needle penetration into heartwood (Matheny et al., 2015). Probes were individually calibrated before installation in order to ensure the accuracy of StWC estimates from raw readings of dielectric permittivity (ϵ). For this, *Q. ilex* trees were felled outside the experimental plots and cut into 15-cm-long stem segments of similar diameter to the selected trees. Bark was sanded in non-crooked sections before segments were immersed into deionized water overnight. Volume of stem segments was estimated the next day by Archimedes' principle to the nearest 0.1 ml, and probes were installed afterwards. Three parallel holes were radially drilled into the stem using a customized drill guide where bark was previously sanded. To ensure a tight contact between stem and needle, the drill bit diameter was equal to that of the probe needle. A dead-blow hammer was used to carefully push the needles into the holes, and non-caustic silicone was applied to seal the stem-probe interface. After probe installation, stem segments were weighted to the nearest 0.1 g near water saturation point and as stems dehydrated at a room temperature of approximately 20°C, while ϵ was recorded every minute with a data logger (Campbell CR3000, Campbell Scientific Ltd, Shephed, UK). Stem segments were disconnected from the logger to be weighted, twice per day during the first week of dehydration and then once per day during the second week. After 2 weeks, probes and silicon were detached and weighted to correct weight readings of the stem segment. Dry weight was determined after four additional weeks in a dry oven at 60°C until constant weight, and StWC (kg/m^3) was determined according to:

$$\text{StWC} = \frac{\text{Fresh weight} - \text{Dry weight}}{\text{Volume}} \quad (2)$$

The linear relationship between StWC and the mean $\sqrt{\epsilon}$ recorded during the hour before and after the fresh weight reading was established according to manufacturer indications:

$$\text{StWC} = a \sqrt{\epsilon} + b \quad (3)$$

where a and b are the slope and intercept of this linear relationship, respectively. A preliminary linear model showed that the intercept of this relationship significantly varied with each probe ($p < .001$, $n = 9$). Considering probe as a random (intercept) factor, the slope of this relationship was significant ($p < .001$), whereas the interaction $\sqrt{\epsilon} \times$ probe was not ($p > .1$) denoting equal slopes among probes (Figure S1). The coefficient of determination of the individual fits between StWC and $\sqrt{\epsilon}$ ranged from 0.94 to 0.99. Given the linear relationship between $\sqrt{\epsilon}$ and StWC at any time step (Equation (3)), the temporal (sub-daily and seasonal) variation in StWC (ΔStWC) can be estimated by means of the time derivative of $\sqrt{\epsilon}$:

$$\frac{\Delta \text{StWC}}{\Delta t} = \frac{\Delta \text{StWC} \Delta \sqrt{\epsilon}}{\Delta \sqrt{\epsilon} \Delta t} = \frac{d \text{StWC} \Delta \sqrt{\epsilon}}{d \sqrt{\epsilon} \Delta t} = a \frac{\Delta \sqrt{\epsilon}}{\Delta t} \quad (4)$$

In this way, it is possible to determine ΔStWC rather than absolute values from ϵ readings, thereby avoiding the use of random (unknown) intercept values. After calibration, probes were installed in the field following the protocol described above. Probes were installed in selected trees at approximately 0.5 m above the soil and on the north face of the stem to avoid direct solar radiation. Readings were performed every 30 minutes and recorded with a data logger (model CR1000, Campbell Scientific Ltd, Sheshed, UK). More than 2 years of data are shown here, from sensor installation in December 2016 (DOY 341) until DOY 365 in 2018. Because ϵ can be affected by temperature (Chanzy, Gaudu, & Marloie, 2012), two additional probes were installed in dead stems to evaluate the potential effect of the temperature sensitivity of ϵ ($\alpha = \Delta \epsilon / \Delta T$; $^{\circ}\text{C}^{-1}$) on estimates of ΔStWC . For this, α was estimated on a daily basis as the slope between ϵ and dead stem temperature (T_{STEM} ; $^{\circ}\text{C}$) recorded by the probe, and the relationship between α and mean daily ϵ was evaluated across the surveyed period. A direct sub-daily relationship between ϵ and T_{STEM} in dead stems was observed during summer ($\epsilon < 4-5$) resulting in roughly constant and positive temperature sensitivity of ϵ ($\alpha \approx 0.04^{\circ}\text{C}^{-1}$, Figure S2). As dead stems rehydrated during wetter months, the sub-daily relationship between ϵ and T_{STEM} became non-significant, and even inverted at the highest range of ϵ ($> 8-9$) resulting in negative α (down to $-0.03^{\circ}\text{C}^{-1}$). This variable pattern of α in relation to ϵ throughout the year and the lack of overlap between ϵ ranges measured in dead ($\epsilon < 10$) and living ($\epsilon > 10$) trees prevented any temperature-correction of ϵ to refine ΔStWC estimates.

2.3 | Gradients in water potential and stem water content

To calculate gradients in Ψ on seasonal and sub-daily bases, seven and six Ψ measurement campaigns were performed encompassing the dry season of 2017 (DOYs 171, 185, 234, 251, 268, 284 and 298) and 2018 (DOYs 171, 187, 133, 256, 276 and 297), respectively. In each campaign, leaf Ψ was measured at predawn and midday (Ψ_{PD} and Ψ_{MD} , respectively) in trees equipped with GS3 probes, except on DOY 268 of 2017 and DOY 256 of 2018, when uniquely Ψ_{PD} was measured. Leaf Ψ was measured with a pressure chamber (PMS1000, PMS Instruments, Corvallis, OR) on freshly excised leafy shoots sampled at similar tree height and solar exposition. Two leafy shoots per tree were sampled, and a third one was added when the first two Ψ readings differed by more than 0.2 MPa. In cases of missing Ψ data for a particular tree at a given date (9 cases for a total of 104; 8 trees \times 13 dates), treatment mean values were applied. Seasonal $\Delta \Psi$ was estimated as the reduction in Ψ_{PD} relative to the spring maxima (-0.45 MPa; Limousin et al., 2012). Ideally, stem Ψ readings would be necessary to estimate C_s . Nevertheless, assuming hydraulic equilibrium between leaf and stem Ψ at predawn, the potential bias in seasonal C_s estimates is negligible. Sub-daily $\Delta \Psi$ was calculated as the difference between Ψ_{PD} and

Ψ_{MD} (i.e., the sap flow driving force at midday; Limousin et al., 2009). Hence, sub-daily C_s estimates are likely underestimated as sub-daily shoot $\Delta \Psi$ can be greater than that of the stem, at least during well-hydrated conditions when leaf transpiration is substantial. To evaluate the potential error in sub-daily C_s incurred when using shoot $\Delta \Psi$ instead of stem $\Delta \Psi$, we alternatively used indirect estimates of stem $\Delta \Psi$ to estimate sub-daily C_s , as similarly approached in a modelling exercise at this study site (Salomón et al., 2017). Briefly, leaf and stem Ψ were simultaneously measured at predawn and midday across a drought-stress gradient in a set of *Q. ilex* seedlings (Rodríguez-Calcerrada et al., 2017). Stem Ψ was measured by means of covering leaves with aluminium foil for 1 hr, until hydraulic equilibrium was reached. The ratio between stem and leaf $\Delta \Psi$ along a gradient in Ψ_{PD} observed in *Q. ilex* seedlings was adjusted with a sigmoidal fit and applied here to alternatively estimate sub-daily C_s .

To estimate seasonal and sub-daily C_s following Equation (1), seasonal and sub-daily ΔStWC were estimated for those days in which Ψ measurement campaigns were performed. Seasonal ΔStWC was estimated as the cumulative reduction in StWC relative to the spring maxima registered before summer drought (DOY 156 in 2017 and DOY 151 in 2018). Sub-daily ΔStWC was estimated as the difference between daily minimum StWC registered during high-transpiration hours (from 10:00 to 19:00 hr) minus daily maximum StWC during low-transpiration hours (from 3:00 to 8:00 hr). Additionally, the relationship between seasonal and sub-daily ΔStWC (not restricted to dates of Ψ measurement campaigns) was evaluated across the summer drought periods of 2017 and 2018. To ensure that sub-daily ΔStWC was driven by transpiration, and was not a consequence of water refilling following rain events, days with positive ΔStWC were excluded from analyses. On average, 9% of the days during the dry seasons in 2017 and 2018 were excluded, which is lower than the number of days in which rain was registered (15%).

2.4 | Contribution of stored water to transpiration

Daily transpiration was estimated as the daily cumulative sap flow (kg/day). Sap flow was estimated as the product of sap flux density ($\text{kg cm}^{-2} \text{ hr}^{-1}$) and sapwood area (SA , cm^2). Sap flux density was measured with 20-mm long thermal dissipation probes designed according to Granier (1987) and installed at 1.2 m height. Probes were shielded with aluminium cover to avoid direct solar radiation and rainfall. Sap flux density was recorded every 30 minutes with a data logger (model CR1000, Campbell Scientific)—see Limousin et al. (2009) for further details. Sapwood area was estimated from stem diameter according to the allometric relationship obtained for the study site (Limousin et al., 2009; see Section 4). Daily release of stored water (kg/day) was estimated as the product of sub-daily ΔStWC in absolute terms (kg/m^3) by sapwood volume (m^3). Sapwood volume was estimated assuming tree cylindrical shape as the product of SA by stem height measured in each tree equipped with GS3 probes. Finally, the contribution of stored water to transpiration was estimated as the ratio between daily values of stored water release and transpiration.

2.5 | Sapwood area via electrical resistivity tomography

Electrical resistivity tomography (ERT) was used to quantify SA in a non-destructive manner following the approach described in Benson, Koeser, and Morgenroth (2019). Briefly, 12 nails were inserted around each measured stem at approximately 1 m above the soil until the outer sapwood layer was reached. The geometry of the stem and the location of each nail was recorded using a digital calliper and a measuring tape. Nails were connected with electrodes to a 12-channel resistivity system (PiCUS TreeTronic; Argus Electronic GmbH, Rostock, Germany), and the electrical resistivity (ER) among nails was recorded by the PiCUS software following voltage application and accounting for the geometry of the stem cross section. The resulting tomogram consists of a triangular-based lattice that informs about the spatial variability in ER throughout the stem cross section. The sapwood-heartwood boundary is commonly characterized by a sharp change in water content reflected by a corresponding change in ER, and can therefore be identified as the point of steepest slope of ER along the radial profile of a tomograph (see Figure S3 for an illustration) (Guyot, Ostergaard, Lenkopane, Fan, & Lockington, 2013; Wang, Guan, Guyot, Simmons, & Lockington, 2016). To estimate SA, it is necessary to delineate the boundary between heartwood and sapwood in two dimensions at a fine spatial resolution, which is achieved by means of rotating the surveyed radial profile at a given angle (Benson et al., 2019). For this, optimal bandwidth and the order of the polynomial function (n) used for fitting the gridded data generated by ERT need to be selected a priori. Here, highest R^2 were obtained with a bandwidth of 1 cm and $n = 7$ for all surveyed trees. The R script provided as supplementary material in Benson et al. (2019) was used for SA determination. Total cross-section area derived from tape measurements (including bark) was consistently higher than that obtained via ERT ($16.4 \pm 8.6\%$), likely because the tip of the electrodes were located just beneath the cambium layer so the bark area was unaccounted for in the tomograms. Bark thickness was therefore set to zero in the R script to estimate SA from ERT. Irregularities around the perimeter of the tomography leading to equivocal detection of the sapwood-heartwood boundary were excluded from the ER radial profile.

ERT readings were performed during spring 2019 (DOYs 105–109) in 10 trees per treatment across a range of DBH between 6 and 16 cm. To minimize any potential effect related to sub-daily variation in temperature (Schapman, 2019) and compare SA between treatments, ERT readings were performed around midday and alternatively between C and TE trees. Additionally, the accuracy of this approach was tested by examining the relationship between SA estimated via ERT and visual observation of wet sapwood depth in four freshly cut trees with similar range of DBH located outside the experimental plot (hereafter “validation” trees). Validation trees were cut immediately after ERT readings to visually demarcate sapwood and heartwood, and SA was determined using the image-processing software ImageJ (version 1.52p, FIJI).

2.6 | Data analyses

R software (version 3.6.1) was used for statistical analyses. Cubic smoothing splines were fitted to daily ΔStWC time series to minimize noise in ε readings after rain and at T_{STEM} below 0°C . Seasonal desorption curves exhibited a biphasic shape with different slopes at the beginning and at the end of the dry season (phases I and II hereafter). Comparisons of seasonal C_S between treatments, years and between phases I and II (C_{S_I} and $C_{S_{II}}$ hereafter) were performed by adjusting linear segmented mixed models with the *segmented.lme* function (Muggeo, Atkins, Gallop, & Dimidjian, 2014). Seasonal ΔStWC was determined considering treatment, year, Ψ_{PD} and their interaction as fixed factors, whereas tree was considered as a random slope factor. Treatment and inter-annual differences in the breakpoint along the desorption curve (Ψ_{PD} separating phases I and II) and the difference-in-slope parameters (difference in slope of the desorption curve before and after the breakpoint) were also tested. Random variation in the breakpoint and the difference-in-slope parameters was allowed using a diagonal random effects covariance matrix. Stepwise backward selection was applied for model selection. In this model, the significance of the interaction between Ψ_{PD} and treatment or year denotes different slope of the desorption curve, and hence treatment or inter-annual differences in C_S , respectively.

Sub-daily C_S was estimated as the ratio between sub-daily ΔStWC and $\Delta\Psi$ ($\Psi_{PD} - \Psi_{MD}$) according to Equation (1). To test the effect of TE and Ψ_{PD} on sub-daily C_S , linear mixed models were adjusted considering treatment, Ψ_{PD} and their interaction as fixed factors and tree as a random factor using the *lme* function. The relationship between sub-daily ΔStWC and $\Delta\Psi$ was further examined by a non-linear mixed model using the *nlme* function, as an exponential fit reduced model residual error and AIC relative to the linear fit. The relationship between Ψ_{PD} and $\Delta\Psi$ was analysed likewise. To display non-linear fits, 95% confidence intervals were estimated by first-order Taylor expansion and Monte Carlo simulation (*predictNLS* function in *propagate* library). On a daily basis, treatment differences in Ψ_{PD} , transpiration, water storage release and the contribution of stored water to transpiration were tested with ANOVA. Because of small sample size ($n = 4$), differences with strong ($p < .05$) and moderate ($p < .10$) statistical significance were reported. The allometric relationship between SA and stem diameter was compared between treatments by adjusting log-log linear models and applying stepwise forward selection.

3 | RESULTS

The summer of 2017 was exceptionally dry, with 41.2 mm of rain from early June (DOY 156) to mid-October (DOY 290), when first heavy rains took place (Figure 1a). Summer drought in 2018 was less intense with 97.6 mm of rain from DOY 156 to 279. During these summer drought periods, mean daily air temperature ranged between 13.6 and 30.4°C in 2017, and between 14.9 and 28.7°C in 2018 (Figure 1b). Mean daily T_{STEM} did not differ between treatments throughout the surveyed period, nor during 2017 or 2018 summers ($p > .78$). The more intense summer drought in 2017 relative to 2018

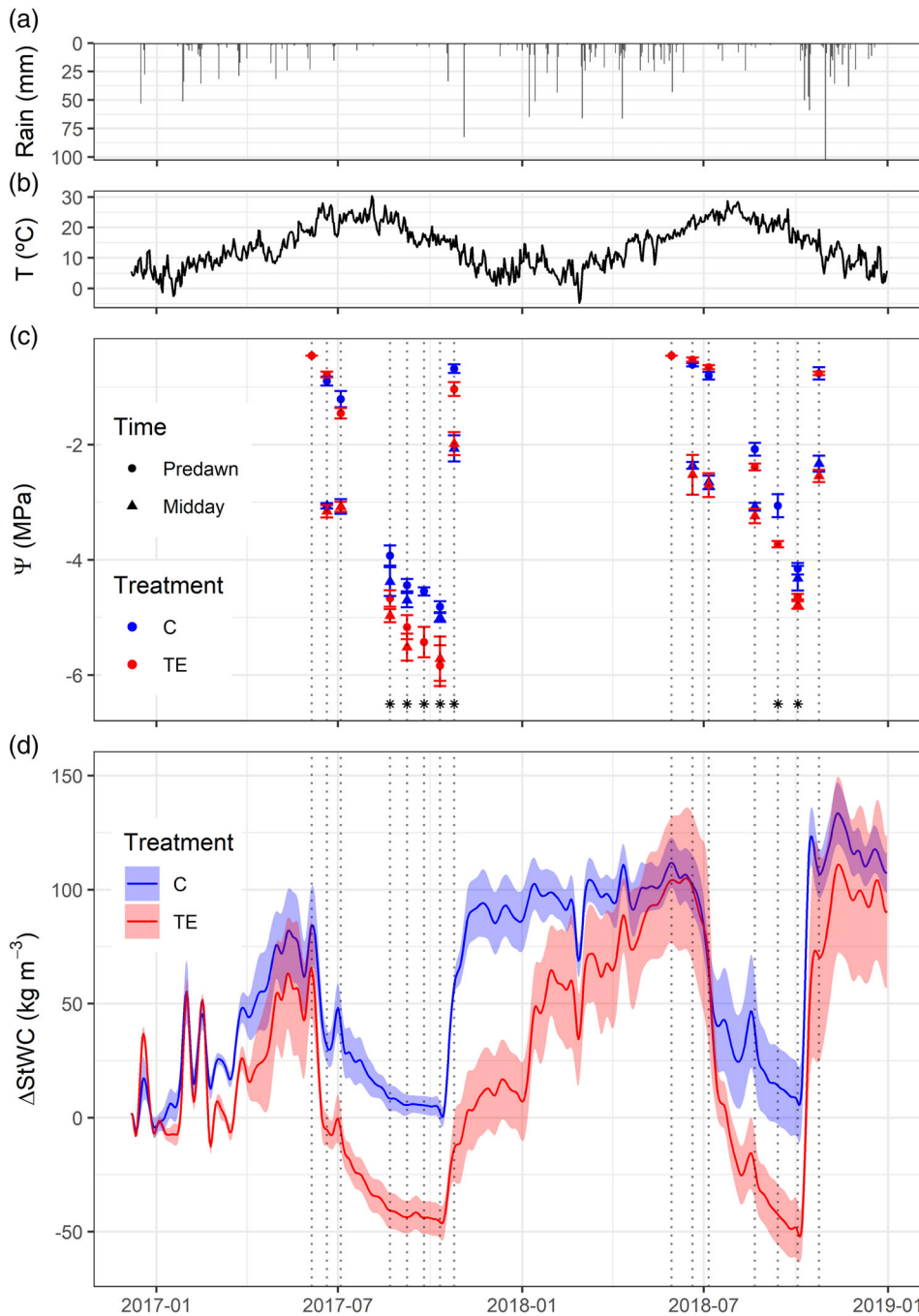


FIGURE 1 Daily values of precipitation (a), mean daily temperature (b), leaf water potential (Ψ) at predawn and midday (c), and variation in stem water content (ΔStWC ; d) since sensor installation in four trees subjected to throughfall exclusion (TE) and control (C) treatment conditions. Mean values \pm SE per treatment ($n = 4$) are shown. Treatment differences in predawn Ψ are shown by asterisks ($p < .05$) [Color figure can be viewed at wileyonlinelibrary.com]

was reflected by the lower yearly minimum Ψ_{PD} in 2017 ($p < .001$). Significant differences in Ψ_{PD} between treatments were observed in both years ($p < .01$; Figure 1c). Minimum Ψ_{PD} in 2017 was -4.8 ± 0.1 and -5.9 ± 0.3 MPa in C and TE trees, respectively, whereas minimum Ψ_{PD} in 2018 was -4.2 ± 0.1 and -4.6 ± 0.1 MPa in C and TE trees, respectively.

3.1 | Seasonal and sub-daily variability in stem water content and hydraulic capacitance

Stem water content consistently decreased during the dry season in 2017 and 2018, reaching lowest values immediately before autumn

first heavy rains (Figure 1d). After 2017 autumn rains, StWC rapidly reached pre-drought levels in C trees, whereas stem refilling was slower in TE trees and additional rain during winter 2018 was necessary to reach pre-drought values. In 2018, stem water refilling following autumn rains was similar between treatments. The larger initial seasonal decline in StWC with decreasing Ψ_{PD} allowed to separate phases I and II of the seasonal desorption curve by their different slopes ($p < .001$, Table 1, Figure 2) and hence capacitances (C_{S_I} and $C_{S_{II}}$, respectively). The breakpoint of the seasonal desorption curve was observed at a Ψ_{PD} of -0.97 and -1.10 MPa in 2017 and 2018, respectively, and did not differ between treatments (Table 1, Figure 2). Above this Ψ_{PD} , the interaction $\Psi_{PD} \times$ treatment was significant ($p < .01$, Table 1), denoting higher C_{S_I} in TE trees ($154 \text{ kg m}^{-3} \text{ MPa}^{-1}$) compared to C ones

TABLE 1 Fixed effects of the segmented mixed linear model for the seasonal relationship between predawn water potential (Ψ_{PD}) and the reduction in stem water content relative to the spring maxima (ΔStWC) in trees subjected to throughfall exclusion (TE) and control conditions across two consecutive years (2017 and 2018)

	Value	SE	p-value
Intercept	-35.79	8.27	.0000
Treatment (TE)	-43.24	10.01	.0050
Left slope			
Ψ_{PD}	7.28	3.21	.0251
$\Psi_{PD} \times \text{Year (2018)}$	10.41	1.46	.0000
Slope change (U)			
U	67.98	17.64	.0002
$U \times \text{Treatment (TE)}$	73.44	24.63	.0036
Breakpoint (G_0)			
G_0	-0.97	0.09	
$G_0 \times \text{Year (2018)}$	-0.13	0.06	.0355

Note: Significant $\Psi_{PD} \times \text{Year}$ interaction indicates different slope of the relationship between Ψ_{PD} and ΔStWC at the left-hand side of the breakpoint in Figure 2, and therefore different stem capacitance between years during phase II of the desorption curve ($C_{S_{II}}$). Significant U indicates significant change in slope at the breakpoint (difference in slope of the desorption curve before and after the breakpoint), so that C_{S_I} is higher than $C_{S_{II}}$. Significant $U \times \text{Treatment}$ interaction indicates different change in the slope between treatments at the right-hand side of the breakpoint in Figure 2, and therefore higher C_{S_I} in TE trees. The breakpoint G_0 differed between years. The standard deviation of the random effects considering a diagonal random effects covariance matrix was 7.470, 0.310, 0.002 and 19.71 for Ψ_{PD} , U, G_0 and the residual, respectively.

(80 kg m⁻³ MPa⁻¹). On the contrary, the slope of the desorption curve below the breakpoint substantially decreased (Figure 2), and the interaction $\Psi_{PD} \times \text{treatment}$ became not significant, denoting low and similar $C_{S_{II}}$ between treatments (< 20 kg m⁻³ MPa⁻¹). Unexpectedly, a larger reduction in seasonal ΔStWC was observed in 2018 than in 2017 (Figure 1d), resulting in a significantly higher $C_{S_{II}}$ in 2018 relative to 2017 (18 and 7 kg m⁻³ MPa⁻¹, respectively; Figure 2). The interaction $\Psi_{PD} \times \text{treatment} \times \text{year}$ was not significant above or below the breakpoint point, denoting consistency in the inter-annual treatment comparisons of both C_{S_I} and $C_{S_{II}}$.

Sub-daily C_s estimated using shoot Ψ measurements to calculate the midday sap flow driving force ($\Delta\Psi = \Psi_{PD} - \Psi_{MD}$) was 19.73 \pm 5.92 kg m⁻³ MPa⁻¹. When indirect estimates of stem $\Delta\Psi$ were applied (see Figure S4a), sub-daily C_s increased to 33.38 \pm 6.70 kg m⁻³ MPa⁻¹. Independently of the $\Delta\Psi$ applied for calculation, sub-daily C_s did not differ between treatments nor across a Ψ_{PD} gradient ($p > .1$). Accordingly, parameters of the non-linear relationship between sub-daily ΔStWC and shoot $\Delta\Psi$ did not differ between treatments (Figure 3). Sub-daily ΔStWC increased (in absolute terms) with $\Delta\Psi$, which was in turn determined by Ψ_{PD} (inset Figure 3), and exhibited highest values when $\Delta\Psi$ was above 2 MPa, before drought stress exacerbated. Figure S4b shows these relationships when indirect estimates of stem $\Delta\Psi$ were used for calculation. Seasonal and

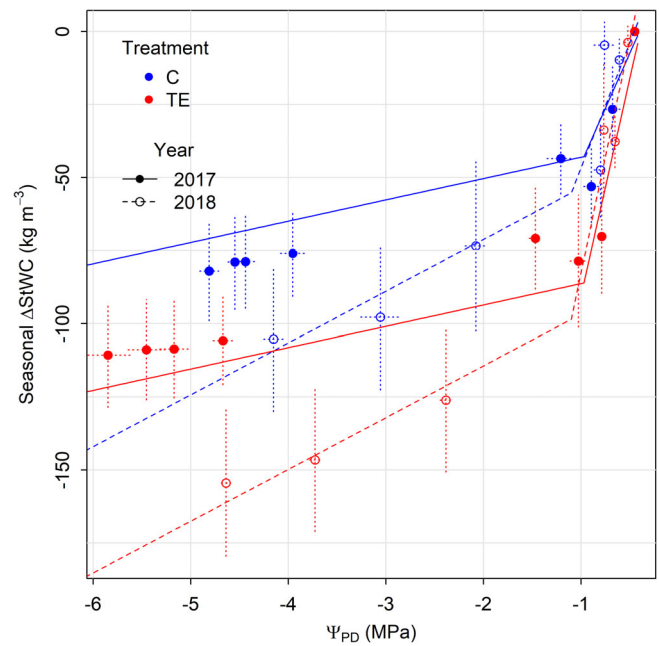


FIGURE 2 Seasonal relationship between predawn water potential (Ψ_{PD}) and the cumulative reduction in stem water content (ΔStWC) during summer drought relative to the spring maxima measured in trees subjected to throughfall exclusion (TE) and control (C) conditions during two consecutive summers. Points illustrate mean values \pm SE per treatment ($n = 4$) and measurement campaign. Seasonal desorption curves were adjusted with segmented mixed models. The slopes of these curves above and below the breakpoint equal stem hydraulic capacitance during the first and second phase of the seasonal desorption curve, respectively [Color figure can be viewed at wileyonlinelibrary.com]

sub-daily ΔStWC were not linearly related (Figure 4a). Sub-daily ΔStWC (in absolute terms) did not peak at the start of the dry season, but after mild dehydration, when the evaporative demand was likely higher. Highest sub-daily ΔStWC , ranging between 25–35 and 18–25 kg/m³, were reached in early summer of 2017 and 2018, respectively (Figure 4a, b). Following seasonal dehydration, sub-daily ΔStWC progressively decreased down to 5 kg/m³ for both years (Figure 4a, c and d). Overall, sub-daily ΔStWC was not significantly affected by TE. Mean values of sub-daily ΔStWC were moderately higher in TE trees uniquely in sparse days along phase I of the seasonal desorption curve (e.g., Figure 4b, $p < .1$).

3.2 | Daily transpiration and release of stored water

Figure 5 illustrates dynamics in transpiration, stored water release and the contribution of stored water to transpiration along the summer course, since StWC maxima until first autumn heavy rains. Transpiration maxima was close to 10 and 12 kg/day in 2017 and 2018, respectively. Minimum transpiration rates down to 2 kg/day were reached at the end of both dry seasons (Figure 5a, b). Release of stored water was substantially smaller, ranging from maxima of 2–3 kg/day during spring

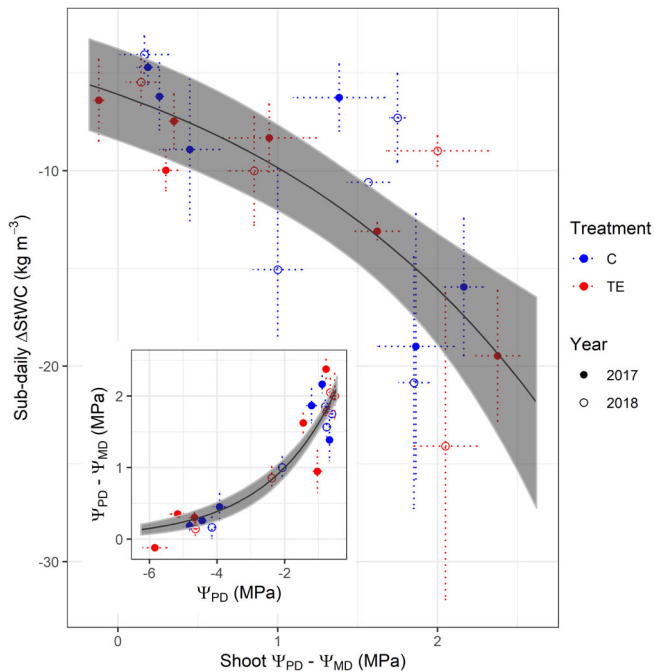


FIGURE 3 Relationship between midday sap flow driving force (difference between predawn and midday shoot water potential, $\Delta\Psi = \Psi_{PD} - \Psi_{MD}$) and sub-daily variation in stem water content (ΔStWC). The inset illustrates the relationship between $\Delta\Psi$ and Ψ_{PD} . Measurements were performed in trees subjected to throughfall exclusion (TE) and control (C) conditions during two consecutive summers. Points illustrate mean values \pm SE per treatment ($n = 4$) and measurement campaign. Fit displayed was adjusted with a non-linear model pooling data from different treatments and years [Color figure can be viewed at wileyonlinelibrary.com]

and early summer, down to 0.2 kg/day at the end of the dry season (Figure 5c, d). The contribution of stored water to transpiration did not exhibit any clear temporal pattern, with mean values fluctuating around 0.1 (Figure 5e, f). Transpiration tended to be higher in C than TE trees when Ψ_{PD} was high, although this difference was not significant (Figure 6a). Transpiration decreased with decreasing Ψ_{PD} ($p < .001$), with the interaction $\Psi_{PD} \times \text{treatment}$ being significant ($p < .05$), reflecting that TE trees were able to maintain similar transpiration rates at more negative Ψ_{PD} . The release of stored water to the transpiration stream decreased with Ψ_{PD} ($p < .001$; Figure 6b). It tended to be higher in TE trees, although this difference was not significant when considering the whole surveyed period; differences were uniquely observed in early summer of 2018 (Figure 5d). The daily contribution of stored water to transpiration was not related to Ψ_{PD} (Figure 6c). Again, although this ratio tended to be higher in TE trees, differences were not significant considering the whole surveyed period and were uniquely and sparsely observed during the summer of 2018 (Figure 5f).

3.3 | Sapwood area

The range of electrical resistivity for each surveyed stem is displayed in Figure 7. Overall, individual ER minima and maxima largely

varied independently of the treatment. Minimum ER values were mostly below 100 Ωm , and maximum ER rarely exceeded 1,600 Ωm . The slope and intercept of the log-log linear regression between stem diameter (D) and SA did not differ between treatments ($p > .05$; Figure 8). Pooling trees from C and TE treatments, the coefficients a and b of the allometric relationship between SA (cm^2) and D (cm):

$$SA = a D^b \quad (5)$$

were 0.682 and 1.911, respectively. These coefficients did not differ significantly from those previously obtained at this site, in which SA area was visually determined (Limousin et al., 2009). The coefficient of determination between SA estimated visually and via ERT in validation trees was 0.96, with ERT estimates being higher than those visually determined (Figure S5).

4 | DISCUSSION

4.1 | Methodological considerations to quantify stem water content

Methodological constraints to accurately monitor StWC in vivo have limited our knowledge about spatial and temporal dynamics in C_s and its response to stress elicitors, although it might be of primary relevance within the context of drought-driven tree mortality (Körner, 2019; Martínez-Vilalta et al., 2019). Frequency domain reflectometry is becoming increasingly applied to the detriment of time domain reflectometry due to its comparable potential to provide continuous and long-term data on StWC in a non-destructive manner for a relatively lower cost (e.g., Beedlow, Waschmann, Lee, & Tingey, 2017; Hao et al., 2013; Matheny et al., 2015; Oliva Carrasco et al., 2015; Saito et al., 2016). The need for accurate FDR probe calibration in the wood medium is, however, important to highlight. Some earlier works have seen an agreement between laboratory and factory calibration before applying parameters given by the manufacturers to estimate StWC from ϵ readings (e.g., Hao et al., 2013; Oliva Carrasco et al., 2015). Nevertheless, these probes are originally designed and calibrated to measure soil water content and the relationship between $\sqrt{\epsilon}$ and water content could largely differ according to the medium (Matheny et al., 2015; Saito et al., 2016; Wulschleger, Hanson, & Todd, 1996). Here, a constant slope of the relationship between $\sqrt{\epsilon}$ and gravimetric StWC allowed reliable evaluation of ΔStWC at different timescales, but random variation of the intercept prevented the estimation of absolute StWC values. Custom probe shortening might have affected the parameters defining the $\sqrt{\epsilon}$ -StWC relationship (Matheny et al., 2015). Further calibration tests across different species and needle lengths would help to evaluate the suitability of fixed parameters given by the manufacturers to estimate StWC under different experimental conditions. Moreover, as calibration tests are, for practical reasons, generally performed during medium dehydration and not rehydration, any potential hysteretic relation between $\sqrt{\epsilon}$ and

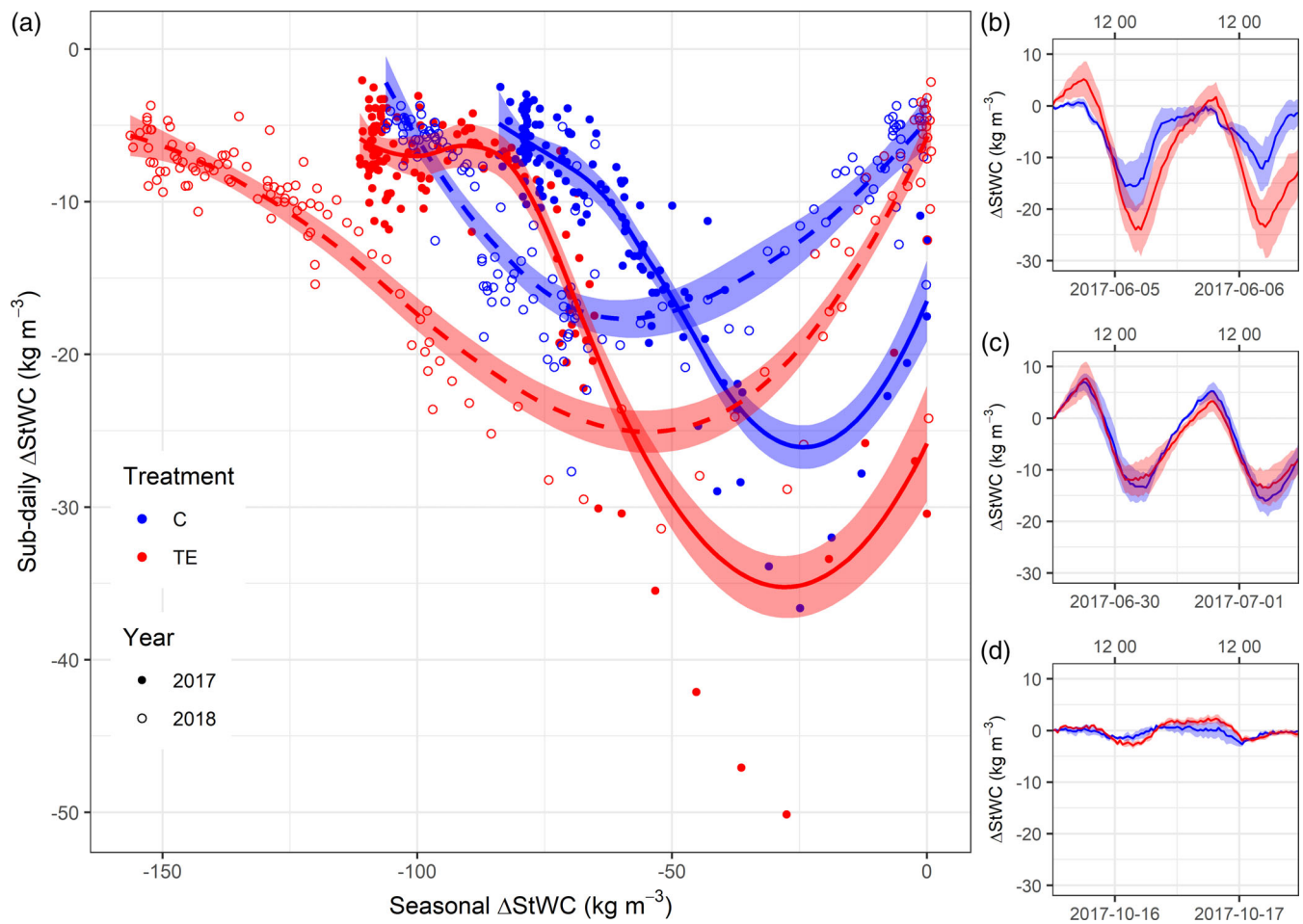


FIGURE 4 Relationship between seasonal (cumulative) and sub-daily variation in stem water content (ΔStWC) during two consecutive summers in trees subjected to throughfall exclusion (TE) and control (C) conditions (a). Three representative 48-hr periods across the 2017 seasonal desorption curve were selected to illustrate sub-daily ΔStWC at an hourly temporal resolution (b–d). Mean values per treatment ($n = 4$) and the smooth curve adjusted by local polynomial regression with its 95% confidence intervals are shown. Solid and dashed lines represent 2017 and 2018 fits, respectively (a). Sub-daily ΔStWC was moderately ($p < .1$) higher in TE trees at the seasonal spring maximum (b), whereas differences became non-significant at the breakpoint of the seasonal desorption curve (c), and at the end of the dry season immediately before first autumn rain (d) [Color figure can be viewed at wileyonlinelibrary.com]

StWC could affect the StWC readings in studies with multiple dehydration-rewetting cycles.

Similarly, T_{STEM} variations may also affect ϵ readings as it occurs with soil temperature variations (Chanzy et al., 2012). Our attempt to account for T_{STEM} effect on StWC estimates by means of monitoring dead trees to avoid transpiration-driven fluctuations in ϵ did not result in a consistent relationship between α and ϵ (Figure S2) that could be extrapolated to living trees. The lack of overlap between ϵ ranges measured in dead and living trees hindered the determination of a reliable α that could be applied in living trees for temperature correction of ϵ across the surveyed period, during which variation in the proportion of free and bound water possibly alters the temperature sensitivity of ϵ . Specific calibration tests applying temperature changes under controlled StWC (Saito et al., 2016) could help to reduce this potential bias in future studies. Further measurement artefacts related to the wounding of stem tissues surrounding the probe needles may also affect ϵ readings. A pioneering study applying time domain

reflectometry reported apparent StWC increases with time since probe installation (Wullschlegel et al., 1996), which could hinder inter-annual comparisons in ΔStWC . It is possible that the comparatively larger ΔStWC (and $C_{s_{10}}$) registered in 2018 than in 2017 was partially explained by a measurement artefact. However, inter-annual variation in ΔStWC could also be explained by different meteorological conditions. Smaller ΔStWC in 2017 was caused by the inter-annual difference in spring StWC maxima, which was lower in 2017 than in 2018, with the summer StWC minima being similar during both years (Figure 1d). This observation could also suggest that stem water reservoirs were not fully replenished in 2017 before the onset of the seasonal desorption curve. Incomplete stem refilling in 2017 could be possibly attributed to relatively drier winter and spring months (Figure 1a). At this time, cumulative rain previous to the spring StWC maxima in 2017 was 39, 35, 45, 53 and 51% of that registered in 2018 during the 1-, 2-, 3-, 4- and 5-month period preceding spring StWC maxima, respectively.

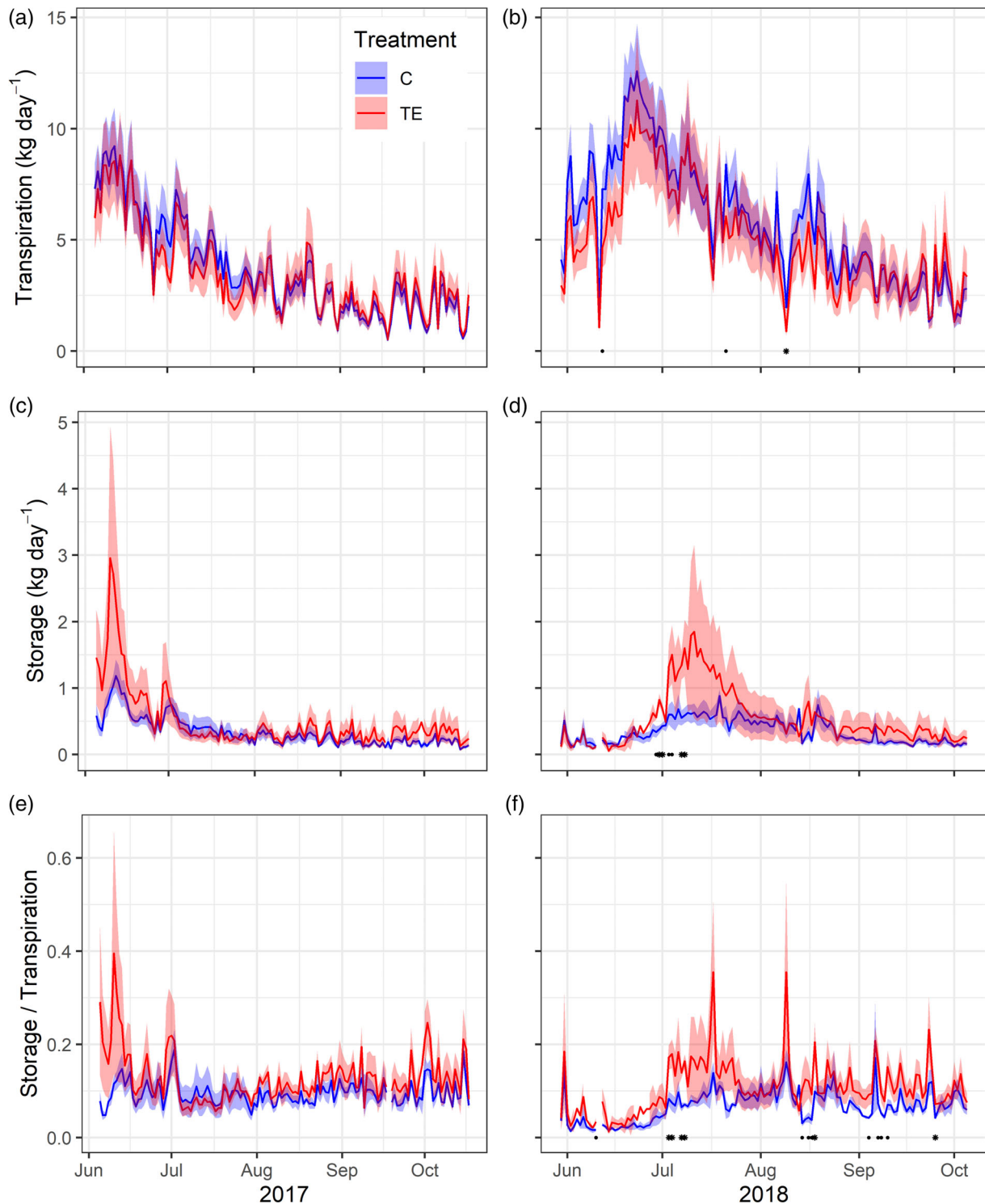


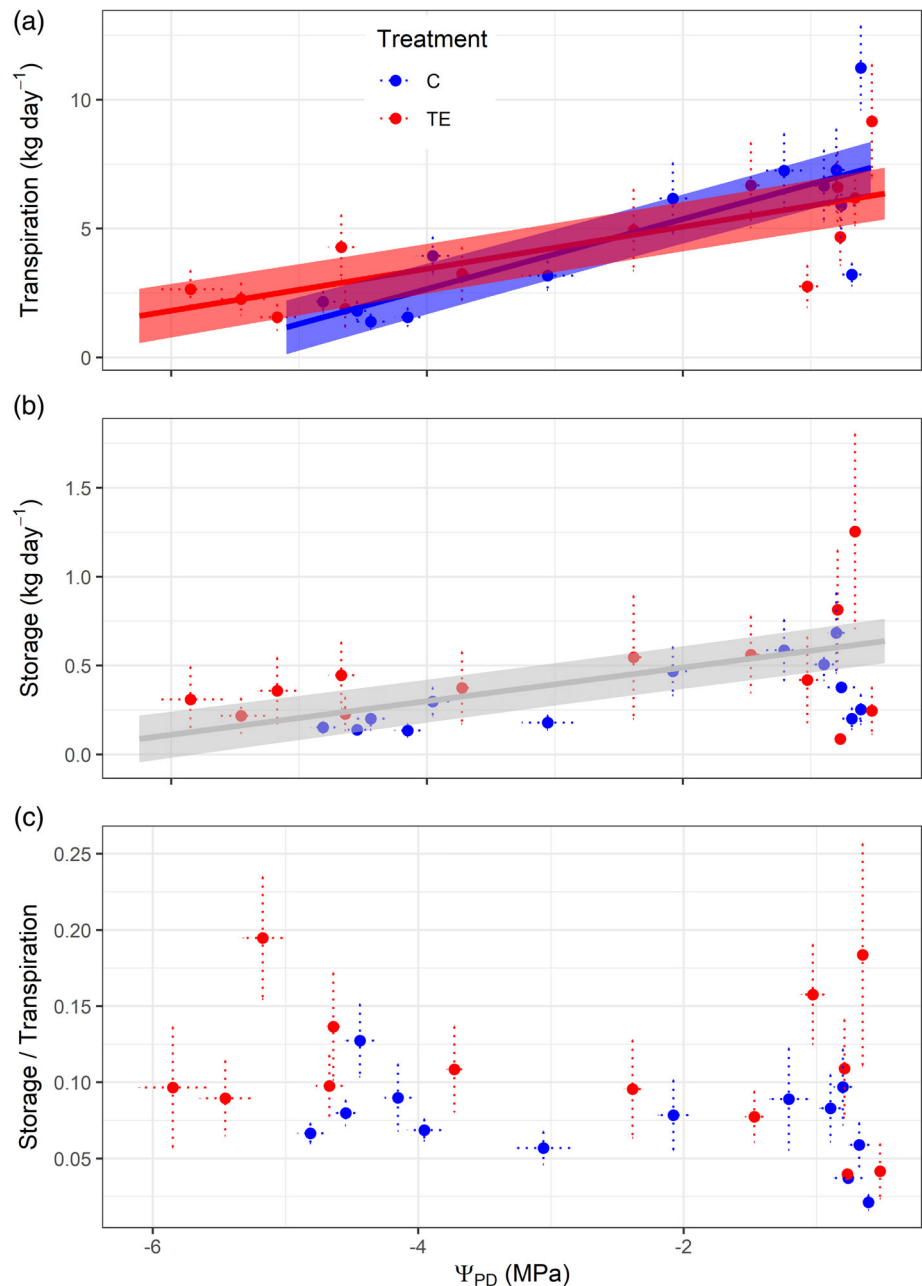
FIGURE 5 Daily values of transpiration (a and b), release of stored water (c and d) and the contribution of stored water to transpiration (e and f) in trees subjected to throughfall exclusion (TE) and control (C) conditions during two consecutive summers (2017 and 2018). Mean values \pm SE per treatment ($n = 4$) are shown. Treatment differences at α level of 0.05 and 0.1 are shown by asterisks and points, respectively [Color figure can be viewed at wileyonlinelibrary.com]

4.2 | Seasonal and sub-daily variation in stem water content and capacitance

Stem water pools were largely depleted during summer drought, as similarly observed in several species subjected to water deficit

(Beedlow et al., 2017; Hao et al., 2013; Hernández-Santana & Martínez-Fernández, 2008; Matheny et al., 2015). The seasonal desorption curve exhibited a steep decrease under well-hydrated conditions, which flattened as drought-stress exacerbated. Therefore, C_s decreased along the dry season, with the breakpoint of the desorption

FIGURE 6 Relationships between predawn water potential (Ψ_{PD}) and daily transpiration (a), stored water release (b), and the contribution of stored water to transpiration (c). Data were obtained from trees subjected to throughfall exclusion (TE) and control (C) conditions during two consecutive summers. Mean values \pm SE per treatment ($n = 4$) and measurement campaign are shown. Regression lines shown when the relationship with Ψ_p was significant ($p < .05$). Different lines per treatment shown when the interaction $\Psi_{PD} \times$ treatment was significant [Color figure can be viewed at wileyonlinelibrary.com]



curve being observed at Ψ_{PD} between -0.97 and -1.10 MPa (Figure 2). Capillary water is mostly released at water potentials above -0.2 MPa (Tyree & Yang, 1990) and largely depleted below -0.5 MPa (Pratt & Jacobsen, 2017; Tyree & Ewers, 1991), which is in accordance with the negative pressure required to drain capillaries as calculated from Laplace's law (Knipfer et al., 2017). Therefore, capillary water might be physiologically irrelevant during phase I of the desorption curve (Ψ_{PD} between -0.45 and -1.10 MPa) and C_{S-I} could be primarily attributed to elastic living cells. The subsequent reduction in C_S during phase II might result from the limited contribution of largely depleted elastic pools together with a small capacitive water release from vessel embolism given the remarkable embolism resistance of *Q. ilex*, with P_{12} values down to -4.93 MPa

(Lobo et al., 2018). Remarkably, the breakpoint of the desorption curve closely matched the threshold for stem growth interruption imposed by water deficit at the study site ($\Psi_{PD} = -1.1$ MPa; Lempereur et al., 2015) and was not modified by TE. Stem growth being a turgor-driven process, it requires sufficient turgor pressure in the cambial cells for cell division and enlargement (Hsiao & Xu, 2000; Steppe et al., 2015). Stem living cells during phase I were probably still sufficiently hydrated to build-up the turgor pressure above the yield threshold, while the large depletion of water pools during phase II of this curve constrained cambial turgor below this yield threshold. The coincidence of these two Ψ_{PD} thresholds for stem growth and stem hydraulic capacitance suggests that stem elastic water pools are responsible for both the stem capacitive water

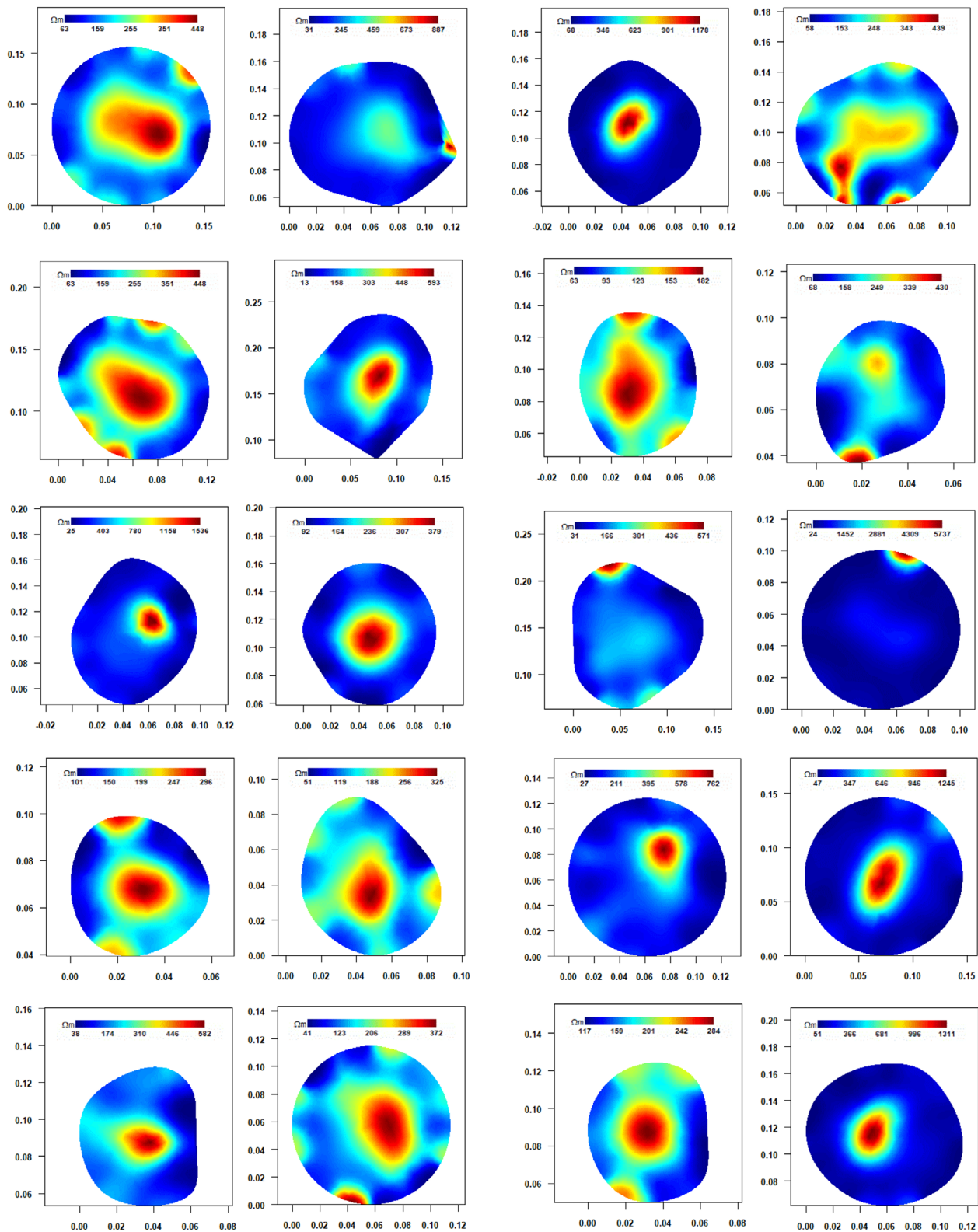


FIGURE 7 Electrical resistivity tomographies of 10 trees subjected to control conditions (two columns on the left-hand side) and permanent throughfall exclusion (two columns on the right-hand side). Horizontal and vertical axes in each tomograph illustrate the dimension of the stem cross-section in m. The range of electrical resistivity (ER, Ωm) is depicted by the colour bar. In some cases, irregularities around the perimeter of the cross section resulted in high ER. These irregularities were excluded from the ER radial profile to locate the heartwood-sapwood boundary. Note that images directly generated by the PICUS software do not illustrate the actual range of ER values, but maximize the colour contrast towards the centre of the tomography by adjusting the range of the colour map [Color figure can be viewed at wileyonlinelibrary.com]

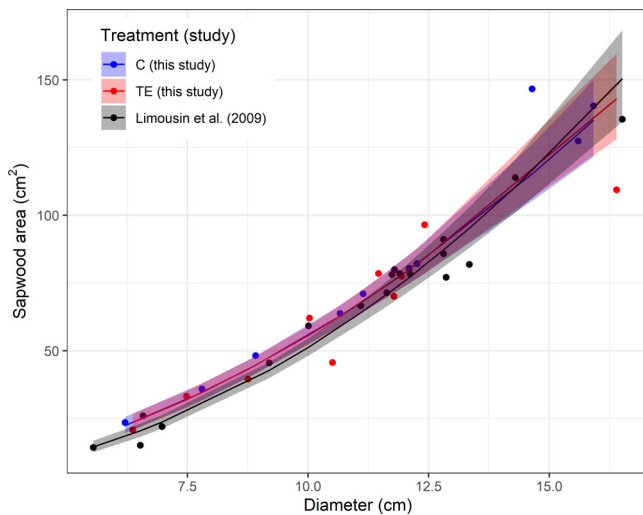


FIGURE 8 Relationship between stem diameter and sapwood area measured via electrical resistivity tomography in trees subjected to throughfall exclusion (TE) and control (C) conditions. Solid lines and polygons represent the mean \pm SE of the exponential fits. Black points display the diameter-sapwood area relationship previously observed at the site (Limousin et al., 2009) for comparison purposes [Color figure can be viewed at wileyonlinelibrary.com]

release along phase I and the turgor pressure that drives cell wall yielding during growth.

Stem capacitance is commonly estimated as the initial slope of the desorption curve. Initial capacitance in *Q. ilex* was below $160 \text{ kg m}^{-3} \text{ MPa}^{-1}$, which is consistent with previous reports in evergreen sclerophyll species (Richards et al., 2014), and is lower than the capacitance commonly observed in temperate and tropical trees (Scholz et al., 2011). The shape of the seasonal desorption curve obtained here via FDR was similar to that previously modelled for control trees (cf. Figure 5 in Salomón et al., 2017), using a model that only accounted for the capacitive water release from outer tissues (cambium, phloem and bark). Although FDR cannot discriminate between sapwood and outer tissues as water sources, it would mostly reflect sapwood capacitance as most of the probe needle length (approximately 85%) was in contact with sapwood. Modelled $C_{S,I}$ of outer tissues in control trees ($62 \text{ kg m}^{-3} \text{ MPa}^{-1}$; Salomón et al., 2017) was lower than measured $C_{S,I}$ here ($80 \text{ kg m}^{-3} \text{ MPa}^{-1}$), suggesting a greater capacitance of sapwood tissues on a volume basis, as similarly observed in Neotropical savanna trees (Scholz et al., 2007).

As initially hypothesized, permanent throughfall exclusion increased seasonal C_S . However, and contrary to our expectations, differences were observed during phase I of the desorption curve, when trees were still well-hydrated, instead of during phase II, when reliance on stored water might play a more important role in maintaining xylem hydraulic functionality. These results suggest that capacitive water release to limit Ψ reductions represents a secondary strategy to face drought in *Q. ilex*, as this drought-tolerant species is highly resistant to drought-driven embolism, with P_{50} values of -7.13 MPa (Lobo et al., 2018). Contrarily to drought-avoidant species, the significance of C_S in drought-tolerant species such as *Q. ilex* might

be more important to maximizing carbon gain during well-hydrated conditions than to dampening Ψ reductions under drought stress. According to this idea, the use of stem water pools increased carbon gain by 18% in Douglas-fir trees (Phillips et al., 2003) and by up to 12% in tropical forests (Bartlett, Detto, & Pacala, 2019), which can be achieved by enlarging periods of transpiration at sub-daily and seasonal timescales (Bartlett et al., 2019; Beedlow et al., 2017; Goldstein et al., 1998). Moreover, TE trees exhibited a more gradual decline in transpiration with decreasing Ψ_{PD} (Figure 6a). This pattern is consistent with the reduced sensitivity of transpiration to short-term fluctuations in atmospheric vapour pressure deficit (VPD) and soil moisture (SM) following long-term reductions in soil water availability (Grossiord et al., 2018). Lower sensitivity of transpiration to VPD and SM allows TE trees to maintain transpiration across a wider gradient of Ψ_{PD} but comes at the cost of reduced annual tree transpiration. Transpiration of our sample of trees was 8 and 16% lower in TE relative to C trees in 2017 and 2018, respectively, but a significant reduction of transpiration of approximately 23% has been observed over the long-term course of the experiment and related to a reduction of the trees' leaf area (Gavinet, Ourcival, & Limousin, 2019; Limousin et al., 2009). Reduced sensitivity of transpiration to VPD can also limit water loss under conditions of very high temperature and evaporative demand, which are not necessarily optimal in terms of photosynthetic carbon gain (e.g., Drake et al., 2018). Therefore, although TE limits tree transpiration and carbon gain in absolute terms following leaf area reductions (Limousin et al., 2009), greater $C_{S,I}$ together with reduced sensitivity of transpiration to VPD and SM could better couple transpiration dynamics with optimal photosynthetic conditions (Phillips et al., 2003), and thereby improve whole-tree water use efficiency.

Mean sub-daily C_S estimates increased from 20 to $33 \text{ kg m}^{-3} \text{ MPa}^{-1}$ when direct shoot $\Delta\Psi$ measurements and indirect estimates of stem $\Delta\Psi$ were used for calculation, respectively, thereby highlighting the need of direct stem Ψ measurements in future research to more accurately estimate sub-daily C_S . Regardless of the $\Delta\Psi$ used for calculation, sub-daily C_S was similar between treatments and across the surveyed Ψ_{PD} gradient. Similar sub-daily C_S concomitant with increased seasonal $C_{S,I}$ in TE trees suggests that, although the difference between sub-daily StWC maximum and minimum remained homeostatic between treatments, daily refilling along phase I of the seasonal desorption curve was more limited in TE trees (Figure 4b), eventually resulting in a greater cumulative reduction in StWC at a longer (seasonal) temporal scale. Furthermore, although the contribution of stored water to daily transpiration tended to be higher in TE, especially during the summer 2018 (Figure 5e, f), treatment differences were not significant for most of the surveyed period, as similarly observed for ponderosa pines across an aridity gradient (Maherali & DeLucia, 2001). It is important to note, however, that the small sample size in this study ($n = 4$) limits the statistical power of tests applied to detect any treatment effect. Daily stored water release and transpiration decreased proportionally with decreasing Ψ_{PD} , resulting in a roughly constant contribution of stored water to transpiration of around 10% (Figure 6), a value within the lower range

of observations made for other species (from 10 to 50%; reviewed by Scholz et al., 2011). A sustained contribution of sapwood water pools to daily transpiration contrasts with the modelled result that the contribution to transpiration of stored water from outer tissues increased with decreasing Ψ_{PD} (Salomón et al., 2017). This apparently contradictory observation could be explained by the spatial location of the different water reservoirs along the stem radial profile. Sapwood water pools are intimately connected to conducting xylem vessels, possibly acting as immediate water sources to fulfil transpiration needs in a proportional manner. Contrastingly, outer tissues located over the cambium layer are indirectly connected to xylem vessels via radial ray parenchyma, possibly acting as delayed reservoirs with lower initial capacitance but able to remain hydrated for longer periods, hence increasing its contribution to transpiration as drought stress progresses.

4.3 | Hydraulic capacitance in relation to hydraulic allometry

Stem water storage capacity, reliance on stored water to fulfil transpiration needs and C_S are relatively plastic traits related to sapwood volume and tree allometry (Scholz et al., 2011). Allometric adjustments to chronic water limitation, assessed along aridity gradients, favour biomass allocation to conducting and storing sapwood to the detriment of transpiring leaves (Maherali & DeLucia, 2001; Martínez-Vilalta et al., 2009; Martin-StPaul et al., 2013; Rosas et al., 2019). Accordingly, intra-specific comparisons in two conifer species have shown greater C_S in drier sites, consistent with larger sapwood thickness, number of tree rings in sapwood, percentage of tree rings in sapwood, and a (non-significant) tendency of higher sapwood thickness relative to stem diameter (Barnard et al., 2011). In view of these observations, we hypothesized that potential changes in C_S could be attributed to a structural acclimation of the sapwood depth in response to long-term water limitation. To test this hypothesis, we performed *in vivo* measurements of SA via ERT in 10 trees from each treatment. The allometric relationship between SA and stem diameter did not differ between treatments (Figure 8) refuting our hypothesis. This comparison, however, should be taken with caution due to unaccounted sources of variation in ER (e.g., electrolyte content, wood density; Bär, Hamacher, Ganthaler, Losso, & Mayr, 2019), illustrated here by large differences in the ER range registered among stems (Figure 7). Unexplained variability in ER may shift the point of steepest change in ER along the stem radial profile, commonly resulting in overestimation of SA via ERT (Benson et al., 2019; Wang et al., 2016), as similarly observed here in the four validation trees cut outside the experimental plots. Nevertheless, this bias did not significantly affect the relationship between stem diameter and SA relative to that visually obtained considering a larger sample size ($n = 18$; Limousin et al., 2009), confirming the validity of allometric extrapolations applied at the site.

Differences in C_S were observed during phase I of the seasonal desorption curve, when elastic water pools might be the largest

source of capacitive water release. Regardless of similar SA between treatments, elastic water pools could be larger in TE trees, as suggested by the lower wood density previously observed in branches of TE trees (Limousin et al., 2010). Wood density is directly related to Young's modulus of elasticity (Niklas & Spatz, 2010). Therefore, less dense wood with lower Young's modulus undergoes greater elastic deformation for a given pressure, hence enabling greater release and refill of water for a given change in xylem Ψ . This is the reason why wood density is inversely related to C_S (McCulloh et al., 2014; Meinzer et al., 2009). We further speculate that reductions in the leaf-to-sapwood area ratio (LA/SA) could be related to the observed increase in $C_{S,L}$. Previous studies have shown that leaf biomass production in the TE plot was significantly and consistently reduced by 23% (Gavinet et al., 2019) and that the leaf area index was also lower because increased leaf life span or decreased leaf mass per area did not compensate for the lower leaf production (Limousin et al., 2012). Significant reductions in LA/SA were thus observed at the branch level (Limousin et al., 2010; Limousin et al., 2012) and confirmed here at the whole tree level considering homeostatic SA measured via ERT and LA reductions observed in previous studies at the site. The mechanism linking LA/SA ratios with C_S remains, however, unclear and dedicated experiments should be performed to address this hypothetical relation.

Further research in wood anatomy and tree water content regulation under drought stress (Knipfer et al., 2019; Martínez-Vilalta et al., 2019) could help to more accurately discriminate how stem capacitive water sources are preferentially used during drought stress, and to better understand the underlying link between C_S and the regulation of water potential and carbon and water exchange. More long-term data on stem water pools, C_S and allometric adjustments applying non-destructive techniques across different species would be necessary to evaluate the generality of the pattern observed here and advance knowledge on hydraulic acclimation strategies across plant functional types. Research in drought-prone Mediterranean regions could be particularly informative as the largest body of research in stem water pools has so far focused on more mesic (temperate and tropical) species, whose response to severe drought events could substantially differ from that of drought-tolerant ones.

ACKNOWLEDGMENTS

We are grateful to Karim Piquemal for assistance during calibration, installation and maintenance of GS3 probes, to Vito Muggeo for his valuable support on the statistical analyses of mixed segmented models, and to Jonas von der Crone for his support and guidance in the analyses of ERT data. We thank two anonymous reviewers for their thoughtful comments on an earlier version of this manuscript. The Puéchabon experimental site belongs to the SOERE F-ORE-T, which is supported annually by Ecofor, Allenvi and the French national research infrastructure ANAEE-F, and the OSU-OREME of Montpellier. This project has received funding from the FWO and the European Union's Horizon 2020 research and innovation programme under the Marie Skłodowska-Curie grant agreement no 665501 granted to R. L. S.

CONFLICT OF INTEREST

The authors declare no conflict of interest.

ORCID

Roberto L. Salomón  <https://orcid.org/0000-0003-2674-1731>

REFERENCES

- Bär, A., Hamacher, M., Ganthaler, A., Losso, A., & Mayr, S. (2019). Electrical resistivity tomography: Patterns in *Betula pendula*, *Fagus sylvatica*, *Picea abies* and *Pinus sylvestris*. *Tree Physiology*, 39, 1262–1271.
- Barnard, D. M., Meinzer, F. C., Lachenbruch, B., McCulloh, K. A., Johnson, D. M., & Woodruff, D. R. (2011). Climate-related trends in sapwood biophysical properties in two conifers: Avoidance of hydraulic dysfunction through coordinated adjustments in xylem efficiency, safety and capacitance. *Plant, Cell & Environment*, 34, 643–654.
- Bartlett, M. K., Detto, M., & Pacala, S. W. (2019). Predicting shifts in the functional composition of tropical forests under increased drought and CO₂ from trade-offs among plant hydraulic traits. *Ecology Letters*, 22, 67–77.
- Beedlow, P. A., Waschmann, R. S., Lee, E. H., & Tingey, D. T. (2017). Seasonal patterns of bole water content in old growth Douglas-fir (*Pseudotsuga menziesii* [Mirb.] Franco). *Agricultural and Forest Meteorology*, 242, 109–119.
- Benson, A. R., Koeser, A. K., & Morgenroth, J. (2019). Estimating conductive sapwood area in diffuse and ring porous trees with electronic resistance tomography. *Tree Physiology*, 39, 484–494.
- Chanzy, A., Gaudu, J. C., & Marloie, O. (2012). Correcting the temperature influence on soil capacitance sensors using diurnal temperature and water content cycles. *Sensors*, 12, 9773–9790.
- Choat, B., Brodribb, T. J., Brodersen, C. R., Duursma, R. A., López, R., & Medlyn, B. E. (2018). Triggers of tree mortality under drought. *Nature*, 558, 531–539.
- Domec, J.-C., & Gartner, B. L. (2001). Cavitation and water storage capacity in bole xylem segments of mature and young Douglas-fir trees. *Trees*, 15, 204–214.
- Drake, J. E., Tjoelker, M. G., Vårhammar, A., Medlyn, B. E., Reich, P. B., Leigh, A., ... Barton, C. V. M. (2018). Trees tolerate an extreme heatwave via sustained transpirational cooling and increased leaf thermal tolerance. *Global Change Biology*, 24, 2390–2402.
- Gavin, J., Ourcival, J., & Limousin, J. (2019). Rainfall exclusion and thinning can alter the relationships between forest functioning and drought. *New Phytologist*, 223, 1267–1279.
- Goldstein, G., Andrade, J. L., Meinzer, F. C., Holbrook, N. M., Cavelier, J., Jackson, P., & Celis, A. (1998). Stem water storage and diurnal patterns of water use in tropical forest canopy trees. *Plant, Cell & Environment*, 21, 397–406.
- Granier, A. (1987). Evaluation of transpiration in a Douglas-fir stand by means of sap flow measurements. *Tree Physiology*, 3, 309–320.
- Grossiord, C., Sevanto, S., Limousin, J. M., Meir, P., Mencuccini, M., Pangle, R. E., ... McDowell, N. G. (2018). Manipulative experiments demonstrate how long-term soil moisture changes alter controls of plant water use. *Environmental and Experimental Botany*, 152, 19–27.
- Guyot, A., Ostergaard, K. T., Lenkopane, M., Fan, J., & Lockington, D. A. (2013). Using electrical resistivity tomography to differentiate sapwood from heartwood: Application to conifers. *Tree Physiology*, 33, 187–194.
- Hao, G. Y., James, K. W., Michele Holbrook, N., & Goldstein, G. (2013). Investigating xylem embolism formation, refilling and water storage in tree trunks using frequency domain reflectometry. *Journal of Experimental Botany*, 64, 2321–2332.
- Hernández-Santana, V., & Martínez-Fernández, J. (2008). TDR measurement of stem and soil water content in two Mediterranean oak species. *Hydrological Sciences Journal*, 53, 921–931.
- Hsiao, T. C., & Xu, L. K. (2000). Sensitivity of with of roots versus leaves to water stress: Biophysical analysis and relation to water. *Journal of Experimental Botany*, 51, 1595–1616.
- Hudson, P. J., Limousin, J. M., Krofcheck, D. J., Boutz, A. L., Pangle, R. E., Gehres, N., ... Pockman, W. T. (2018). Impacts of long-term precipitation manipulation on hydraulic architecture and xylem anatomy of piñon and juniper in Southwest USA. *Plant, Cell & Environment*, 41, 421–435.
- Knipfer, T., Cuneo, I. F., Mason, E. J., Reyes, C., Brodersen, C. R., & McElrone, A. J. (2017). Storage compartments for capillary water rarely refill in an intact woody plant. *Plant Physiology*, 175, 1649–1660.
- Knipfer, T., Reyes, C., Earles, J. M., Berry, Z. C., Johnson, D., Brodersen, C. R., & McElrone, A. J. (2019). Spatiotemporal coupling of vessel cavitation and discharge of stored xylem water in a tree sapling. *Plant Physiology*, 179, 01303.2018.
- Körner, C. (2019). No need for pipes when the well is dry—A comment on hydraulic failure in trees. *Tree Physiology*, 39, 695–700.
- Kramer, P. J. (1937). The relation between rate of transpiration and rate of absorption of water in plants. *American Journal of Botany*, 24, 10–15.
- Lamy, J.-B., Delzon, S., Bouche, P. S., Alia, R., Vendramin, G. G., Cochard, H., & Plomion, C. (2014). Limited genetic variability and phenotypic plasticity detected for cavitation resistance in a Mediterranean pine. *New Phytologist*, 201, 874–886.
- Lempereur, M., Martin-StPaul, N. K., Damesin, C., Joffre, R., Ourcival, J.-M., Rocheteau, A., & Rambal, S. (2015). Growth duration is a better predictor of stem increment than carbon supply in a Mediterranean oak forest: Implications for assessing forest productivity under climate change. *New Phytologist*, 207, 579–590.
- Limousin, J. M., Longepierre, D., Huc, R., & Rambal, S. (2010). Change in hydraulic traits of Mediterranean *Quercus ilex* subjected to long-term throughfall exclusion. *Tree Physiology*, 30, 1026–1036.
- Limousin, J. M., Rambal, S., Ourcival, J. M., & Joffre, R. (2008). Modelling rainfall interception in a mediterranean *Quercus ilex* ecosystem: Lesson from a throughfall exclusion experiment. *Journal of Hydrology*, 357, 57–66.
- Limousin, J. M., Rambal, S., Ourcival, J. M., Rocheteau, A., Joffre, R., & Rodriguez-Cortina, R. (2009). Long-term transpiration change with rainfall decline in a Mediterranean *Quercus ilex* forest. *Global Change Biology*, 15, 2163–2175.
- Limousin, J. M., Rambal, S., Ourcival, J. M., Rodríguez-Calcerrada, J., Pérez-Ramos, I. M., Rodríguez-Cortina, R., ... Joffre, R. (2012). Morphological and phenological shoot plasticity in a Mediterranean evergreen oak facing long-term increased drought. *Oecologia*, 169, 565–577.
- Lobo, A., Torres-Ruiz, J. M., Burlett, R., Lemaire, C., Parise, C., Francioni, C., ... Delzon, S. (2018). Assessing inter- and intraspecific variability of xylem vulnerability to embolism in oaks. *Forest Ecology and Management*, 424, 53–61.
- Magnani, F., Grace, J., & Borghetti, M. (2002). Adjustment of tree structure in response to the environment under hydraulic constraints. *Functional Ecology*, 16, 385–393.
- Maherali, H., & DeLucia, E. H. (2001). Influence of climate-driven shifts in biomass allocation on water transport and storage in ponderosa pine. *Oecologia*, 129, 481–491.
- Martinez-Vilalta, J., Anderegg, W. R. L., Sapes, G., & Sala, A. (2019). Greater focus on water pools may improve our ability to understand and anticipate drought-induced mortality in plants. *New Phytologist*, 223, 22–32.
- Martinez-Vilalta, J., Cochard, H., Mencuccini, M., Sterck, F., Herrero, A., Korhonen, J. F. J., ... Zweifel, R. (2009). Hydraulic adjustment of Scots pine across Europe. *New Phytologist*, 184, 353–364.
- Martin-StPaul, N. K., Limousin, J.-M., Vogt-Schilb, H., Rodríguez-Calcerrada, J., Rambal, S., Longepierre, D., & Misson, L. (2013). The temporal response to drought in a Mediterranean evergreen tree: Comparing a regional precipitation gradient and a throughfall exclusion experiment. *Global Change Biology*, 19, 2413–2426.

- Matheny, A. M., Bohrer, G., Garrity, S. R., Morin, T. H., Howard, C. J., & Vogel, C. S. (2015). Observations of stem water storage in trees of opposing hydraulic strategies. *Ecosphere*, 6, 165.
- McCulloh, K. A., Johnson, D. M., Meinzer, F. C., & Woodruff, D. R. (2014). The dynamic pipeline: Hydraulic capacitance and xylem hydraulic safety in four tall conifer species. *Plant, Cell & Environment*, 37, 1171–1183.
- Meinzer, F. C., James, S. A., & Goldstein, G. (2004). Dynamics of transpiration, sap flow and use of stored water in tropical forest canopy trees. *Tree Physiology*, 24, 901–909.
- Meinzer, F. C., James, S. A., Goldstein, G., & Woodruff, D. (2003). Whole-tree water transport scales with sapwood capacitance in tropical forest canopy trees. *Plant, Cell & Environment*, 26, 1147–1155.
- Meinzer, F. C., Johnson, D. M., Lachenbruch, B., McCulloh, K. A., & Woodruff, D. R. (2009). Xylem hydraulic safety margins in woody plants: Coordination of stomatal control of xylem tension with hydraulic capacitance. *Functional Ecology*, 23, 922–930.
- Meinzer, F. C., Woodruff, D. R., Domec, J.-C., Goldstein, G., Campanello, P. I., Gatti, M. G., & Villalobos-Vega, R. (2008). Coordination of leaf and stem water transport properties in tropical forest trees. *Oecologia*, 156, 31–41.
- Mencuccini, M. (2003). The ecological significance of long-distance water transport: Short-term regulation, long-term acclimation and the hydraulic costs of stature across plant life forms. *Plant, Cell and Environment*, 26, 163–182.
- Muggeo, V. M. R., Atkins, D. C., Gallop, R. J., & Dimidjian, S. (2014). Segmented mixed models with random change points: A maximum likelihood approach with application to treatment for depression study. *Statistical Modelling*, 14, 293–313.
- Niklas, K. J., & Spatz, H.-C. (2010). Worldwide correlations of mechanical properties and green wood density. *American Journal of Botany*, 97, 1587–1594.
- Oliva Carrasco, L., Bucci, S. J., Di Francescantonio, D., Lezcano, O. A., Campanello, P. I., Scholz, F. G., ... Goldstein, G. (2015). Water storage dynamics in the main stem of subtropical tree species differing in wood density, growth rate and life history traits. *Tree Physiology*, 35, 354–365.
- Phillips, N. G., Ryan, M. G., Bond, B. J., McDowell, N. G., Hinckley, T. M., & Cermak, J. (2003). Reliance on stored water increases with tree size in three species in the Pacific Northwest. *Tree Physiology*, 23, 237–245.
- Poorter, H., Niklas, K. J., Reich, P. B., Oleksyn, J., Poot, P., & Mommer, L. (2012). Biomass allocation to leaves, stems and roots: Meta-analysis of interspecific variation and environmental control. *New Phytologist*, 193, 30–50.
- Pratt, R. B., & Jacobsen, A. L. (2017). Conflicting demands on angiosperm xylem: Tradeoffs among storage, transport and biomechanics. *Plant Cell and Environment*, 40, 897–913.
- Rambal, S., Lempereur, M., Limousin, J. M., Martin-StPaul, N. K., Ourcival, J. M., & Rodríguez-Calcerrada, J. (2014). How drought severity constrains gross primary production (GPP) and its partitioning among carbon pools in a *Quercus ilex* coppice? *Biogeosciences*, 11, 6855–6869.
- Richards, A. E., Wright, I. J., Lenz, T. I., & Zanne, A. E. (2014). Sapwood capacitance is greater in evergreen sclerophyll species growing in high compared to low-rainfall environments. *Functional Ecology*, 28, 734–744.
- Rodríguez-Calcerrada, J., Jaeger, C., Limousin, J. M., Ourcival, J. M., Joffre, R., & Rambal, S. (2011). Leaf CO₂ efflux is attenuated by acclimation of respiration to heat and drought in a Mediterranean tree. *Functional Ecology*, 25, 983–995.
- Rodríguez-Calcerrada, J., Li, M., López, R., Cano, F. J., Oleksyn, J., Atkin, O. K., ... Gil, L. (2017). Drought-induced shoot dieback starts with massive root xylem embolism and variable depletion of non-structural carbohydrates in seedlings of two tree species. *New Phytologist*, 213, 597–610.
- Rosas, T., Mencuccini, M., Barba, J., Cochard, H., Saura-Mas, S., & Martínez-Vilalta, J. (2019). Adjustments and coordination of hydraulic, leaf and stem traits along a water availability gradient. *New Phytologist*, 223, 632–646.
- Saito, T., Yasuda, H., Sakurai, M., Acharya, K., Sueki, S., Inosako, K., ... Nawata, H. (2016). Monitoring of stem water content of native and invasive trees in arid environments using GS3 soil moisture sensors. *Vadose Zone Journal*, 15, 1–12.
- Salomón, R. L., Limousin, J.-M., Ourcival, J.-M., Rodríguez-Calcerrada, J., & Steppe, K. (2017). Stem hydraulic capacitance decreases with drought stress: Implications for modelling tree hydraulics in the Mediterranean oak *Quercus ilex*. *Plant, Cell & Environment*, 40, 1379–1391.
- Schapman, R. (2019) *How does sapwood area measured with ERT covary with stem growth in Fagus sylvatica L?* (Master thesis dissertation). Ghent University, Belgium.
- Scholz, F. C., Bucci, S. J., Goldstein, G., Meinzer, F. C., Franco, A. C., & Miralles-Wilhelm, F. (2007). Biophysical properties and functional significance of stem water storage tissues in Neotropical savanna trees. *Plant, Cell & Environment*, 30, 236–248.
- Scholz, F. G., Phillips, N. G., Bucci, S. J., Meinzer, F. C., & Goldstein, G. (2011). Hydraulic capacitance: Biophysics and functional significance of internal water sources in relation to tree size. In *Size- and age-related changes in tree structure and function* (pp. 341–361). Dordrecht: Springer.
- Schuldt, B., Knutzen, F., Delzon, S., Jansen, S., Müller-Haubold, H., Burlett, R., ... Leuschner, C. (2016). How adaptable is the hydraulic system of European beech in the face of climate change-related precipitation reduction? *New Phytologist*, 210, 443–458.
- Spalding, E. S. (1905). Mechanical adjustment of the suaharo (*Cereus giganteus*) to varying quantities of stored water. *Bulletin of the Torrey Botanical Club*, 32, 57.
- Steppe, K. (2018). The potential of the tree water potential. *Tree Physiology*, 38, 937–940.
- Steppe, K., De Pauw, D. J. W., Lemeur, R., & Vanrolleghem, A. (2006). A mathematical model linking tree sap flow dynamics to daily stem diameter fluctuations and radial stem growth. *Tree Physiology*, 26, 257–273.
- Steppe, K., Sterck, F., & Deslauriers, A. (2015). Diel growth dynamics in tree stems: Linking anatomy and ecophysiology. *Trends in Plant Science*, 20, 335–343.
- Tyree, M., & Ewers, F. W. (1991). The hydraulic architecture of trees and other woody plants. *New Phytologist*, 119, 345–360.
- Tyree, M. T., & Yang, S. (1990). Water-storage capacity of *Thuja*, *Tsuga* and *Acer* stems measured by dehydration isotherms. *Planta*, 182, 420–426.
- Vergeynst, L. L., Dierick, M., Bogaerts, J. A. N., Cnudde, V., & Steppe, K. (2015). Cavitation: A blessing in disguise? New method to establish vulnerability curves and assess hydraulic capacitance of woody tissues. *Tree Physiology*, 35, 400–409.
- Wang, H., Guan, H., Guyot, A., Simmons, C. T., & Lockington, D. A. (2016). Quantifying sapwood width for three Australian native species using electrical resistivity tomography. *Ecohydrology*, 9, 83–92.
- Waring, R. H., & Running, S. W. (1978). Sapwood water storage: Its contribution to transpiration and effect upon water conductance through the stems of old-growth Douglas-fir. *Plant, Cell and Environment*, 1, 131–140.
- White, D., Beadle, C., Worledge, D., Honeysett, J., & Cherry, M. (1998). The influence of drought on the relationship between leaf and conducting sapwood area in *Trees*, 12, 406.
- Wortemann, R., Herbette, S., Barigah, T. S., Fumanal, B., Alia, R., Ducousso, A., ... Cochard, H. (2011). Genotypic variability and phenotypic plasticity of cavitation resistance in *Fagus sylvatica* L. across Europe. *Tree Physiology*, 31, 1175–1182.
- Wullschlegel, S. D., Hanson, P. J., & Todd, D. E. (1996). Measuring stem water content in four deciduous hardwoods with a time-domain reflectometer. *Tree Physiology*, 16, 809–815.

Zweifel, R., Item, H., & Häslér, R. (2001). Link between diurnal stem radius changes and tree water relations. *Tree Physiology*, 21, 869–877.

SUPPORTING INFORMATION

Additional supporting information may be found online in the Supporting Information section at the end of this article.

How to cite this article: Salomón RL, Steppe K, Ourcival JM, et al. Hydraulic acclimation in a Mediterranean oak subjected to permanent throughfall exclusion results in increased stem hydraulic capacitance. *Plant Cell Environ.* 2020;1–17. <https://doi.org/10.1111/pce.13751>